DOI: 10.26599/FSHW.2026.9251177

Contents lists available at SciOpen

Food Science and Human Wellness

journal homepage: https://www.sciopen.com/journal/2097-0765

China Food Publishing Co.

A New Insight into the Mechanism of DEHP-Induced Hepatotoxicity in Adolescent Mice: Triggering Hepatic Lipid Accumulation by Targeting GRP75-Dependent MAM Formation

Hao Zhang[a], Jia-Gen Cui[a], Bing Sun[a], Yue-Qi Zhang[a], Xue-Nan Li[a, b, c *], Yi Zhao[a, b, c *], Jin-Long Li[a, b, c, *]

[a] *College of Veterinary Medicine, Northeast Agricultural University, Harbin 150030, China*

[b] *Key Laboratory of the Provincial Education Department of Heilongjiang for Common Animal Disease Prevention and Treatment, Northeast Agricultural University, Harbin 150030, China*

[c] *Heilongjiang Key Laboratory for Laboratory Animals and Comparative Medicine, Northeast Agricultural University, Harbin 150030, China*

ABSTRACT: Di(2-ethylhexyl) phthalate (DEHP) is widely acknowledged as a prevalent environmental pollutant, mainly due to its extensive use in plastics. This widespread application has resulted in its presence in air, soil, water, and various food items, as well as in agricultural products and tissues of both humans and animals. With the extensive use of plastic products in daily life, the teenage group is facing an increasing risk of DEHP exposure. However, the mechanism of DEHP-induced liver injury, especially during adolescence, remain unclear. This study utilized metabolomics analysis and molecular biology approaches to explore the effects of DEHP on liver function in adolescent mice. We found that DEHP exposure caused hepatic dysfunction, histopathological abnormalities, and lipid deposition. Metabolomics analysis identified the dysregulation of lipid metabolism, especially the fatty acid pathway. Mechanistically, DEHP and its main metabolite, mono(2-ethylhexyl) phthalate (MEHP) drived the ectopic formation of mitochondrial-associated endoplasmic reticulum membranes (MAMs) by up-regulating glucose-regulated protein 75 (GRP75). Such a process is characterized by a reduced interorganellar contact distance between the endoplasmic reticulum and mitochondria as well as elevated expression of MAM-resident proteins. Notably, overexpression of GRP75 alone recapitulated the lipid accumulation phenotype. Conversely, knockdown of GRP75 attenuated MEHP-induced lipid accumulation in AML12 cells. Moreover, a combination of molecular docking, cellular thermal shift assay (CETSA), and drug affinity responsive target stability (DARTS) assays collectively corroborated the direct physical interaction between MEHP and GRP75. Collectively, our findings demonstrate that DEHP/MEHP disrupts the lipid metabolism regulated by MAM through a GRP75-dependent mechanism, thereby leading to liver steatosis. This study clarified the toxicological mechanisms underlying DEHP-induced hepatic dysfunction in adolescent mice, providing new insights into its health risk assessment and potential intervention strategies.

Keywords: Di (2-ethylhexyl) phthalate; Lipid deposition; Fatty acid metabolism; MAM; GRP75.

1. Introduction

***Corresponding author**
lixuenan@neau.edu.cn (X.N. Li). Zhaoyi@neau.edu.cn (Y. Zhao).
Jinlongli@neau.edu.cn (J.L. Li).

Received 6 September 2025
Received in revised from 20 October 2025
Accepted 5 February 2026

Plastic pollution has evolved into a pressing global environmental challenge. A recent study reveals that people ingest plastic daily[1]. In response to the increasingly serious environmental problems, some developed and developing countries have taken actions and implemented plastic restriction policies[2]. Despite these, the improper disposal and misuse of plastic remain pervasive issues worldwide[3]. Phthalates are a class of plasticizer that are ubiquitous in modern life. These compounds are widely used in polyvinyl chloride products, ranging from food packaging, and medical devices to agricultural films[4-6]. A study has shown that over a period of 30 years from 1990 to 2017, the prevalence and number of cases of non-alcoholic fatty liver disease (NAFLD) among children, adolescents, and young adults have increased[7]. NAFLD is recognized worldwide as the most common chronic liver disease and is increasingly closely related to environmental endocrine disruptors, especially phthalates[8, 9]. Di(2-ethylhexyl) phthalate (DEHP), as one of the most commonly used phthalates, has attracted substantial research attention owing to its potential hepatotoxicity[10, 11]. DEHP bioaccumulates in the human body via the food chain, with dietary ingestion representing the primary route of exposure. Compared with adult livers, the adolescent liver has a weaker homeostatic capacity and is more sensitive to exogenous chemicals, making it more prone to persistent metabolic function disturbances[12, 13]. Of note, children are generally exposed to higher levels of this phthalate than adults[14]. Intrahepatic lipid droplet accumulation is a hallmark of NAFLD, but the molecular mechanism of DEHP-induced intrahepatic lipid droplet accumulation is not yet fully understood. This knowledge gap hinders the development of targeted intervention strategies for environment-driven liver injury.

Hepatic fatty acid metabolic imbalance acts as the pivotal mechanism underlying intrahepatic lipid accumulation, involving the dysregulation of fatty acid uptake, synthesis, oxidation, and export[15, 16]. The dynamic contact regions between mitochondria and the endoplasmic reticulum (ER) are known as mitochondria-associated endoplasmic reticulum membranes (MAMs). These regions facilitate communication between these organelles, coordinating fatty acid synthesis and β-oxidation[17]. Emerging evidence emphasizes that MAM is a key hub for lipid metabolism regulation, influencing lipid accumulation through fatty acid metabolism[18, 19]. Acyl-CoA cholesterol acyltransferase 1 (ACAT1) and diacylglycerol acyltransferase 2 (DGAT2) as key enzymes in the regulation of lipid metabolism[20]. There is a close interaction relationship with MAMs in terms of space and function. ACAT1 and DGAT2, respectively, affect the lipid metabolism balance by regulating cholesterol esterification and triglyceride synthesis[21]. DGAT2 catalyzes the combination of diglycerol esters with fatty acids to form triglycerides (TG), which is the rate-limiting enzyme in the final step of lipid droplet formation and fat storage, especially in the liver[22]. ACAT1 and DGAT2, through the dynamic regulatory network of MAMs, not only affect the lipid metabolism process but also play a key role in NAFLD[23].

Glucose-regulated protein 75 (GRP75) is a chaperone protein anchored to the MAM structure and is related to maintaining the functional coupling of mitochondria and ER[24]. GRP75, as a molecular chaperone, forms complexes with inositol 1,4,5-triphosphate receptor (IP3R) on the ER membrane and voltage-dependent anion channels (VDAC) on the outer mitochondrial membrane, coordinating calcium fluxes and lipid transfer

between organelles[25]. Recent studies have shown that GRP75-mediated MAM dynamically regulates fatty acid β-oxidation (FAO) and adipogenesis by modulating the generation of mitochondria and ER-related lipid droplets[26]. Furthermore, GRP75 has been observed to be overexpressed in chemically induced hepatotoxicity[27]. However, there is still a current knowledge gap regarding whether DEHP disrupts liver lipid metabolism through GRP75-mediated MAM dysfunction.

In this study, we propose that DEHP interferes with the regulation of lipid homeostasis in the liver by influencing the enhancement of MAM through GRP75. Such perturbations shift the balance of fatty acid metabolism to favor adipogenic processes. Our research systematically elucidates the intricate tripartite relationship between DEHP exposure, GRP75-mediated MAM dynamics, and resultant metabolic dysfunction. This discovery has established a new toxicological framework known as "DEHP-GRP75-MAM-fatty acid disorder," offering actionable targets to mitigate metabolic diseases associated with plasticizers. Moreover, the study lays a foundation for addressing fatty liver toxicity and chemical-induced liver injury in NAFLD. This can be achieved through the use of small-molecule modulators of MAM or nutritional interventions aimed at enhancing GRP75 function.

2. Methods and Materials

2.1. Animals

The Northeast Agricultural University's Animal Care and Use Committee has approved all operating procedures for experimental animals (NEAUEC20220341). Three-week-old SPF ICR male mice (Liaoning, China) housed in standard conditions with unrestricted access to food and water. Forty mice were sorted by body weight and randomly divided into two groups, the control group and the experimental group, with 20 mice in each group (Figure 1A). Grouping was conducted by independent people who did not participate in subsequent experiments to control selection bias. The mice were anesthetized and euthanized by cervical dislocation after 28 days of feeding. The liver tissues from the mice were excised during low-temperature dissection and kept at -80℃. The experiment adopted a double-blind design. The drug dosing personnel only knew the animal numbers but not the groups. Sample collection and tissue processing (including pathological staining, qPCR, electron microscopy observation, Western blotting analysis, etc.) were all independently completed by researchers who were unaware of the grouping information. Unblinding and statistical analysis were conducted after all experiments and data collection were completed.

2.2. Reagent and dose selection

The supplier of DEHP was Aladdin Biochemical Technology Co., LTD. (Shanghai, China). It was completely dissolved in corn oil and administered to mice by gavage without causing any additional pathological damage. Since children are usually exposed to higher levels of phthalates than adults, studies have shown that the concentration of DEHP metabolites in the urine of boys is generally higher than that of girls[14, 28]. Three-week-old male ICR mice were selected for the experiment to be exposed to DEHP for 28 consecutive days. An experimental dose of 200 mg/kg/d was employed, determined by considering the need

for standardization in toxicological research, environmental relevance, exposure amplification, the distinctive exposure patterns of adolescents, and the feasibility of mechanistic exploration. The specific justification for this dose is detailed in Supplementary Material 1.1.

2.3. Histopathological examination

The liver sample was sectioned into slices and stained with hematoxylin-eosin (H&E) after being fixed in 4% paraformaldehyde for paraffin embedding. Slices of frozen liver were stained with Oil Red O. Oil Red O-stained slices were subjected to a semi-quantitative examination using ImageJ software.

2.4. Detection of serum biochemical indicators

The levels of liver function test and blood lipid analysis were detected by RT-9200 automatic biochemical analyzer from Shenzhen Mindray Animal Medical Technology Co., Ltd. (Shenzhen, China). The specific indicators are shown in Supplementary Material 1.2.

2.5. Untargeted metabolomics analysis

Metabolite profile analyses were done on liver tissues by APExBIO Technology, LLC (Shanghai, China). Following the previous techniques, sample pretreatment, LC/MS detection, and data analysis were carried out[10]. VIP $\geq$ 1, $P < 0.05$, and FC $\geq$ 2 or FC $\leq$ 0.5 were set as the thresholds for significant differential changes to screen differential metabolites.

2.6. Measurement of FAO and DGAT2

FAO of mouse liver tissue was determined by the FAO colorimetric assay kit (ELAB Science). DGAT2 activity of mouse liver tissue was determined by the Mouse DGAT2 ELISA Kit (Beijing Chenglin Biotechnology). All these detections were performed following instructions.

2.7. Western blotting

The total protein was extracted from the liver tissue, and the western blotting method was performed as previously described[29]. To assess the levels of the target proteins, reference controls GAPDH and β-actin were utilized. Protein bands were visualized with an Amersham Imager 600 (GE, Switzerland), and the densities of the bands were measured using ImageJ software (National Institutes of Health, USA). All antibodies were obtained from Bioss, Affinity and ABclonal (Table S1).

2.8. qRT-PCR analysis

Liver tissues were used to isolate total RNA. mRNA was reverse transcribed and utilized for qRT-PCR following the determination of the RNA samples' concentration and purity. The $2^{-\Delta\Delta Ct}$ method was used to estimate the relative expression level of mRNA. Table S2 lists the primer sequences utilized in this study.

2.9. Ultrastructural analysis

Glutaraldehyde was used to fix the liver tissues, which were then post-fixed, dried, and embedded. The sample slices were then stained. Transmission electron microscopy (Hitachi H7650 Instrument, Tokyo, Japan) was used to analyze the samples. The measurement of mitochondrial-ER spacing was conducted with reference to the methods described in previous literature[30, 31]. For each case, 45 images were considered, and electron microscope images containing clear mitochondria and adjacent ER (mainly rough ER) structures were captured at a magnification of 30,000x. The images were imported into the ImageJ software for analysis. Taking the nearest distinguishable membrane structure between the ER and the outer mitochondrial membrane (OMM) as the object, the vertical spacing was measured. Specifically, for each target mitochondrion, the shortest distance from the ER fragment within a radius of 30 nm around it to the outer membrane of the mitochondrion was measured. And this distance was taken as the mitochondrial-ER spacing at that site.

2.10. Cell culture and treatment

AML12 cells, which were obtained from ATCC (USA), were kept in complete media in a 5% CO_2 atmosphere at 37℃. The complete medium was DMEM/F12 (HyClone, USA) supplemented with 1% insulin-selenium-transferrin (ITS, Gibco, USA), 40 ng/ml dexamethasone (Beyotime, China), 1% penicillin-streptomycin (Gibco, USA), and 10% FBS (Biological Industries, Israel). Mono(2-ethylhexyl) phthalate (MEHP) (AccuStandard Inc., USA) was dissolved in DMSO and incubated with AML12 cells for 24 hours.

2.11. Cell viability assay

AML12 cells were inoculated in 96-well plates and then subjected to MEHP for 24 hours. The CCK-8 solution was added, and it was then incubated for 2 hours. After color development, absorbance was measured at 450 nm with a standard instrument.

2.12. Cell transfection

GRP75 overexpression and knockdown were performed using pcDNA3.1 vectors, pcDNA3.1-GRP75, and siRNA duplexes, respectively. Before transfection, AML12 cells were seeded and cultured in complete media. When the confluency of AML12 cells ranged between 50% and 70%. Lipofectamine 3000 (Invitrogen, USA) was used to transfect the cells for 6 hours. The source of the si-GRP75 (5'-AAGCAAAGGTCCTGGAGAA-3') duplexes was Ruibo Biotechnology Co., LTD (RiboBio, China). PcDNA3.1 vectors and pcDNA3.1-GRP75 overexpression plasmid were designed and synthesized by GenePharma (China).

2.13. Lipid staining with Nile Red

The Nile Red stock solution was stored in the dark, and the working solution (1 μg/mL in PBS) needed to be prepared fresh for each use. After incubating the cells with Nile Red working solution at 37℃ in the dark for 20 minutes, the cells were rinsed three times with PBS. Fluorescence imaging was then performed using a fluorescence microscopy (Leica, Germany).

2.14. Oil Red O staining of AML12 cells

The culture medium was first discarded, and the cells were washed once with PBS. Subsequently, 4% paraformaldehyde solution was added to fix the cells for 10 minutes. After fixation, they were rinsed twice with PBS. Next, the cells were incubated in the oil red O staining working solution for 20 minutes. After staining, the cells were rinsed three times with PBS, and finally, the images were observed and collected under an optical microscope.

2.15. Assessment of mitochondrial membrane potential (MMP)

Cells were stained with JC-1 dye (Beyotime Biotechnology, China) for 20 minutes at 37℃ in order to do MMP analysis. After two JC-1 buffer washes, the cells were given the proper quantity of cell culture media. JC-1 dye builds up in the cytoplasm as monomers and manifests as green fluorescence when the MMP is low. Conversely, when the MMP is high, JC-1 accumulates in the mitochondrial matrix to produce JC-1 aggregates and red fluorescence.

2.16. Mitochondria and ER contact analysis

Cells were labeled with mitochondria using PK Mito Orange (Genvivo Biotech, China) and ER using ER-Tracker Green (Beyotime Biotechnology, China), and then imaged using super-resolution microscopy (NanoTech, China). The co-localization degree of fluorophore mitochondria and ER was quantified using Pearson correlation analysis[32].

2.17. Molecular docking

The primary sequence of GRP75 was obtained from the UniProt database (https://www.uniprot.org/). The 2D structure (SDF format) of MEHP was gained from the PubChem database (https://pubchem.ncbi.nlm.nih.gov/). The molecular docking of MEHP with GRP75 was achieved by the Schrödinger Maestro suite (version 14.3). The 2D structure of MEHP was converted into 3D conformers using LigPrep. Based on the SiteMap prediction, define the binding site and generate the receptor grid surrounding that site. Generate the docking attitude, and then refine it using MM-GBSA calculation to predict the binding free energy.

2.18. Cellular thermal shift assay (CETSA)

AML12 cells were used in the CETSA experiment to evaluate GRP75's thermal stability in the presence of MEHP. After the cells reached 80%–90% confluency, they were removed and resuspended in RIPA buffer containing protease inhibitor cocktail (MCE, USA). After that, the cell suspension was thawed after being flash-frozen in liquid nitrogen. To ensure complete lysis, three freeze-thaw cycles were performed. The resultant lysates were separated from cellular debris by centrifuging them at 20,000 × g for 20 minutes at 4℃. After dividing the supernatants equally between two 1.5 mL tubes, they were incubated for an hour at room temperature with either MEHP (10 μmol/L) or an equivalent volume of DMSO as a vehicle control. Each

mixture was then aliquoted into seven tubes and subjected to heating at specified temperatures ranging from 37 to 67℃ for three minutes, followed by cooling at 4℃ for an additional three minutes. To extract the supernatants containing soluble proteins, the samples were centrifuged again at 20,000 × g for 20 minutes at 4℃. To detect the target protein, these supernatants were then subjected to Western blotting analysis.

2.19. Drug affinity responsive target stability (DARTs)

Take untreated AML12 cells, add them to NP40 lysis buffer containing a 1% protease inhibitor mixture, and lyse at 4℃ for 2 hours. After the lysis is completed, the sample is centrifuged at 4℃ and 12000 × g for 20 minutes. Collect the supernatant and divide the samples of each independent biological repetition into equal parts. Subsequently, 200 μmol/L MEHP or an equal volume of DMSO was added to the equally divided samples, respectively, as controls, and the sample were incubated at room temperature for 1 hour. After incubation, pronase (MCE, USA) was added to each treatment group at ratios of 1:1000, 1:5000, and 1:10000, respectively, and digested at room temperature for 30 minutes. After digestion is completed, immediately add the protein loading buffer and boil at 100℃ for 10 minutes to denature the protein. Finally, the samples were analyzed by Western blotting.

2.20. Protein−protein interaction (PPI) analysis

The String protein interaction database was used to investigate PPI (https://string-db.org/).

2.21. Statistical analysis

The experimental data was gathered from a minimum of three separate tests. For the *in vivo* studies, data (with the exception of Western blot analysis) were obtained from six biological replicates. The data from every study was analyzed using the software packages ImageJ, Origin, and GraphPad Prism 8.0. The mean ± SD is used to express the data. Compared to the CON group that is statistically different, they are denoted by asterisks (*), $P < 0.05$.

3. Results

3.1. DEHP caused liver function damage in mice

To explore the effects of DEHP on liver structure and function, we conducted animal experiments on DEHP exposure (Figure 1A). Initially, we observed the morphological changes of the liver using H&E staining (Figure 1B). H&E staining revealed that the hepatocytes in the CON group were neatly distributed, with normal size and shape. The hepatocytes in the DEHP group were vacuolated and arranged irregularly. Subsequently, we tested the hematology and biochemical indicators. According to the data, DEHP exposure significantly increased the levels of serum AST/ALT, ALP, GLB, ALB/GLB, and CHE when compared to the CON group, as shown in Figure 1C-L. These findings indicate that the structure and function of the liver were impaired after exposure to DEHP.

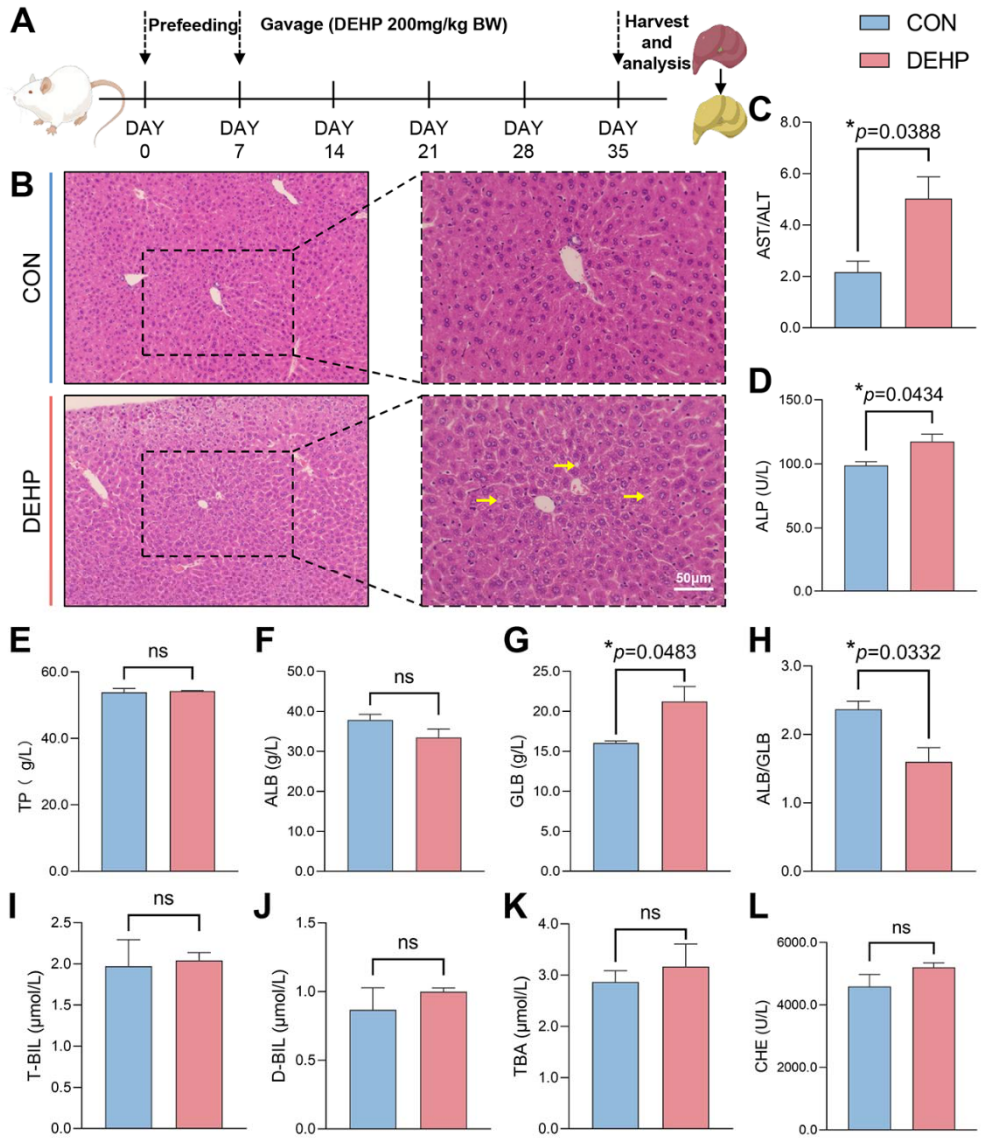

Figure 1. DEHP causes liver function damage in mice. (A) Drug treatment. (B) Histopathology of H&E staining. (C-L) Level of serum AST/ALT, ALP, TP, ALB, GLB, ALB/GLB, T-BIL, D-BIL, TBA, and CHE. *n=6*. Data are presented as the mean ± SD, *n=6*. Symbol for the significance of differences between the CON group and another group: $*P < 0.05$.

3.2. DEHP caused lipid deposition in the liver

To characterize the perturbations in hepatic lipid deposition induced by DEHP exposure, Oil Red O staining was employed in the present study. The findings indicated a minimal degree of lipid accumulation in the CON group, whereas the area exhibiting Oil Red O staining in the DEHP-exposed group demonstrated a significant increase (Figure 2A). The group exposed to DEHP showed a markedly higher number of lipid droplets at the ultramicroscopic level (Figure 2A). Lipid profiling results revealed that serum HDL-C and LDL-C concentrations were elevated in the DEHP-exposed group, with a significant increase in TC levels (Figure 2B-E). Perilipin 2 (PLIN2) is a protein located on the surface of lipid droplets. It plays a crucial role in the formation and stability of lipid droplets, serving as a protein marker for lipid droplets[33]. Heat shock protein 70 (HSC70) is also an essential marker of lipid droplets and plays a key role in lipid droplet metabolism and degradation[34]. We measured the amounts of proteins linked to lipid droplets that were expressed. The expression of PLIN2 significantly increased following DEHP exposure, while the expression of HSC70 did

not change significantly (Figure 2F-H). These results indicated that DEHP caused elevated lipid levels and hepatic lipid deposition in mice.

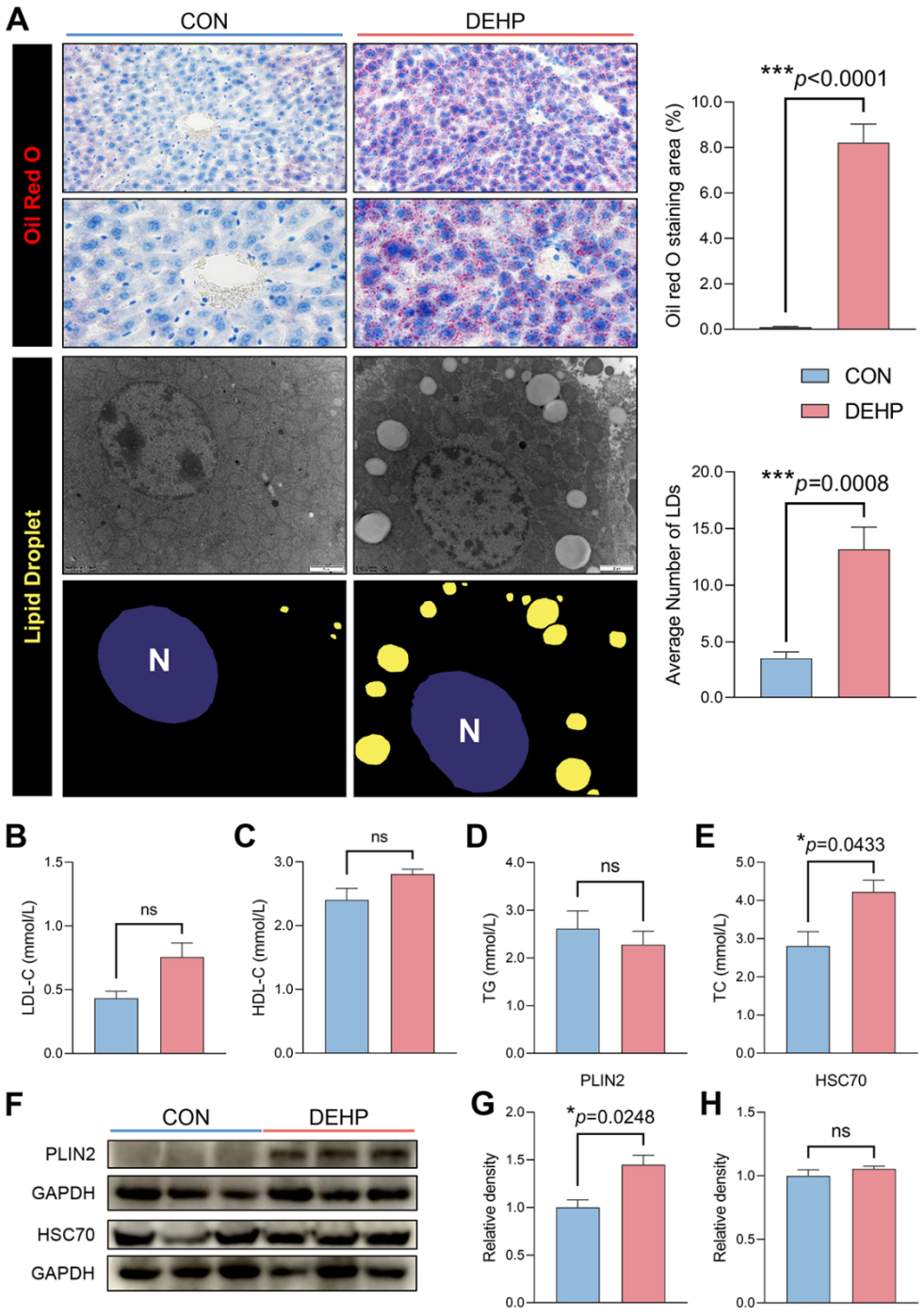

Figure 2. DEHP causes lipid deposition in the liver. (A) Oil Red O staining of liver sections; quantification of Oil Red O staining; transmission electron microscopy of livers, yellow circles represent lipid droplets; quantification of lipid droplets. *n=6*. (B-E) Level of serum LDL-C, HDL-C, TG, and TC. *n=6*. (F) Levels of lipid droplets-related proteins in mouse livers; GAPDH served as loading controls for the total fraction. *n=3*. (G-H) Relative PLIN2 and HSC70 content. *n=3*. Data are presented as the mean ± SD, $n \geq 3$. Symbol for the significance of differences between the CON group and another group: $^{*}P < 0.05$, $^{***}P < 0.001$.

3.3. DEHP caused abnormal fatty acid metabolism in the liver

We used metabolomic techniques to examine the changes in metabolites in the liver following DEHP therapy in order to thoroughly investigate the mechanism of liver damage induced by DEHP. The results of

PLS-DA and the hierarchical clustering heat map revealed significant differences in the composition of the primary liver metabolites between the CON group and DEHP group (Figure 3A-B). The finding indicated that DEHP has a negative impact on the normal physiological processes of the liver. We conducted KEGG pathway enrichment analysis on the differential metabolites. It was found that multiple metabolic pathways in the DEHP group changed, including protein metabolism, carbohydrate metabolism, and lipid metabolism (Figure 3C). The enriched differential metabolites were analyzed, and the results showed that DEHP exposure altered the metabolites related to the glycerol, fatty acid and citrate cycle in the liver of mice (Figure 3C).

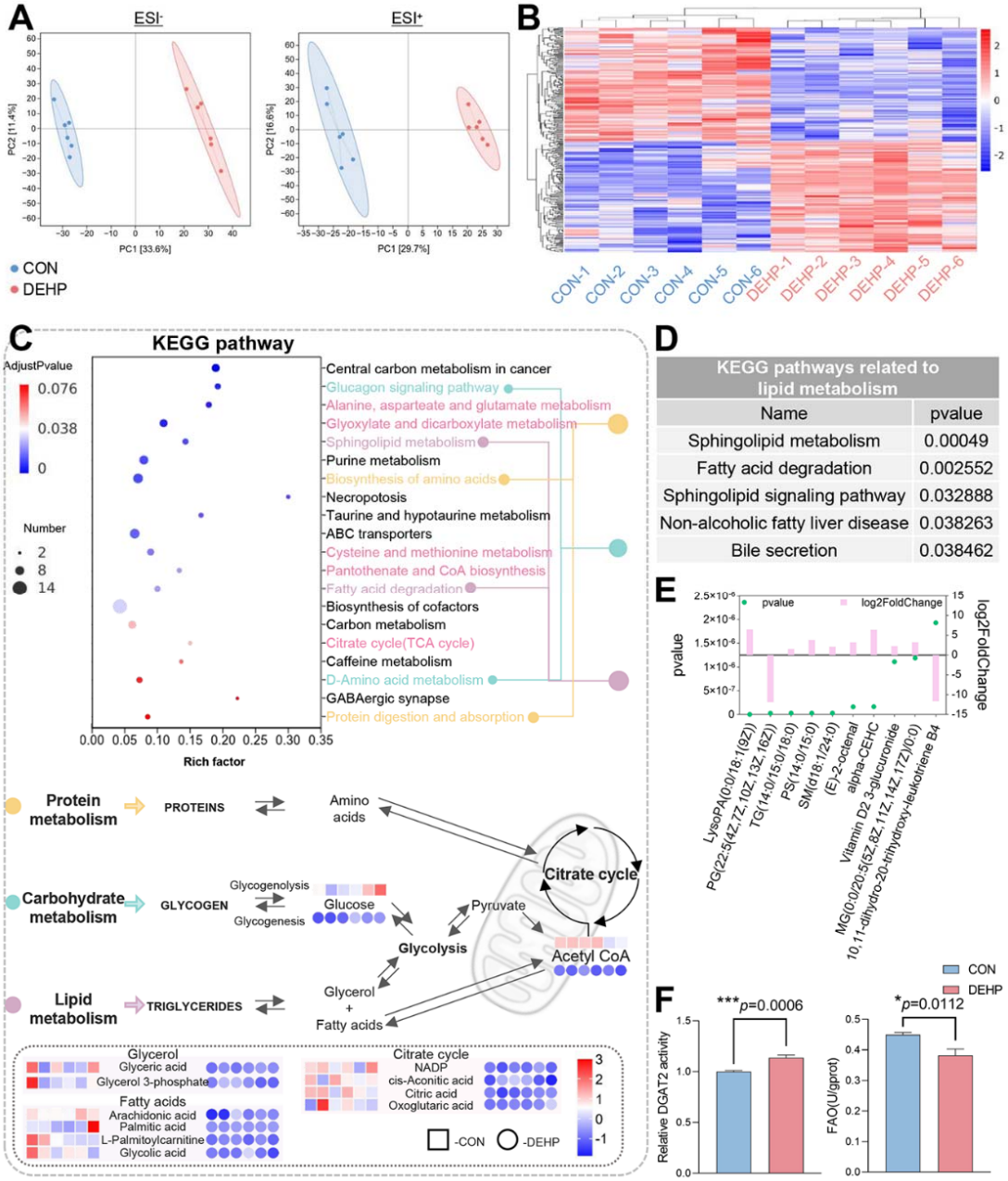

Figure 3. DEHP causes abnormal fatty acid metabolism in the liver. (A) PLS-DA analysis of the liver metabolome. ESI+ indicates the positive ion mode and ESI− indicates the negative ion mode. (B) Hierarchical clustering heat map of differential metabolites. (C) KEGG enrichment analysis of differential metabolites; heat map of differential metabolites related to fatty acid metabolism. (D) KEGG pathways related to lipid metabolism. (E) Top 10 significant changes of lipid metabolites. (F) FAO efficiency and DGAT2 activity in the livers of the mice. $n=6$. Data are presented as the mean ± SD, $n=6$. Symbol for the significance of differences between the CON group and another group: $^{*}P < 0.05$, $^{***}P < 0.001$.

Within the category of lipid metabolism, the five pathways with the highest enrichment levels include sphingolipid metabolism, fatty acid degradation, sphingolipid signaling pathway, NAFLD, and bile secretion (Figure 3D), suggesting that lipid metabolism disorder is the core feature of DEHP hepatotoxicity. To clarify the specific links of lipid disorder, we screened the core differential lipid metabolites. As shown in Figure 3E, among the top ten differential lipid metabolites, TG(14:0/15:0/18:0) and Lysophosphatidic Acid LysoPA(0:0/18:1(9Z)) were significantly upregulated. LysoPA is a key intermediate product in the synthesis of phosphatidic acid (PA) and plays a significant role in the synthesis of TG[35]. In contrast, phosphatidylglycerol PG(22:5(4Z,7Z,10Z,13Z,16Z)), a key phospholipid and cardiolipin precursor for mitochondrial membranes, is down-regulated. This change is often associated with mitochondrial dysfunction and hepatic steatosis[36]. To verify the biological functions of the above metabolomics findings, we examined the activities of key enzymes and metabolic flows. The results showed that after DEHP exposure, the activity of DGAT2 was significantly upregulated, while the efficiency of FAO was significantly weakened (Figure 3F). Fatty acids play a crucial role in liver fatty acid metabolism, triglyceride synthesis and energy homeostasis[15]. Citric acid in mitochondria participates in and promotes the synthesis of fatty acids, and the citrate cycle is the key to generating ATP in the process of fatty acid metabolism[37, 38]. The above results indicate that the lipid deposition in the liver of mice caused by DEHP exposure is closely related to abnormal fatty acid metabolism, with mitochondria potentially playing a significant role.

3.4. DEHP caused the increase in MAM formation in mouse hepatocytes

The metabolism of intracellular fatty acids is highly dependent on the interaction and material transfer between mitochondria and the ER[38, 39]. We detected the mRNA expression levels of proteins related to fatty acid metabolism (SLC25A1, CPT1A, CPT2, MPC1, MPC2, FADS1, FADS2, SCD1, ELOVL1, ELOVL2, ELOVL5, ELOVL6, and ELOVL7) located in mitochondria and ER (Figure 4A-B). According to the qRT-PCR results, DEHP changed the levels of mRNA expression of proteins involved in the metabolism of fatty acids, and this change was associated with mitochondria and ER. MAMs represent a specialized structure that facilitates the connection between ER and mitochondria. It serves as the physical and functional link between mitochondria and the ER and is crucial for intracellular lipid metabolism processes and maintaining cell stability. The results from the electron microscope revealed that the DEHP group's mitochondria and ER were closer together than those of the CON group (Figure 4C-D). The core of MAMs is a conserved multi-protein complex formed by IP3R at the ER. The complex formed by IP3R, GRP75 and VDAC1 plays a crucial role in maintaining the stability of MAM[40]. In the present study, DEHP exposure resulted in a significant upregulation of IP3R, GRP75, and VDAC1 expression (Figure 4E, G). Subsequently, hepatic mitochondrial proteins were isolated to detect the level of GRP75 and VDAC1 proteins. The findings revealed that the expression level of GRP75 increased significantly following DEHP exposure, while there was no significant difference in VDAC1 (Figure 4F, G). These data indicate that the abnormal liver fatty acid metabolism caused by DEHP leads to MAM dysfunction.

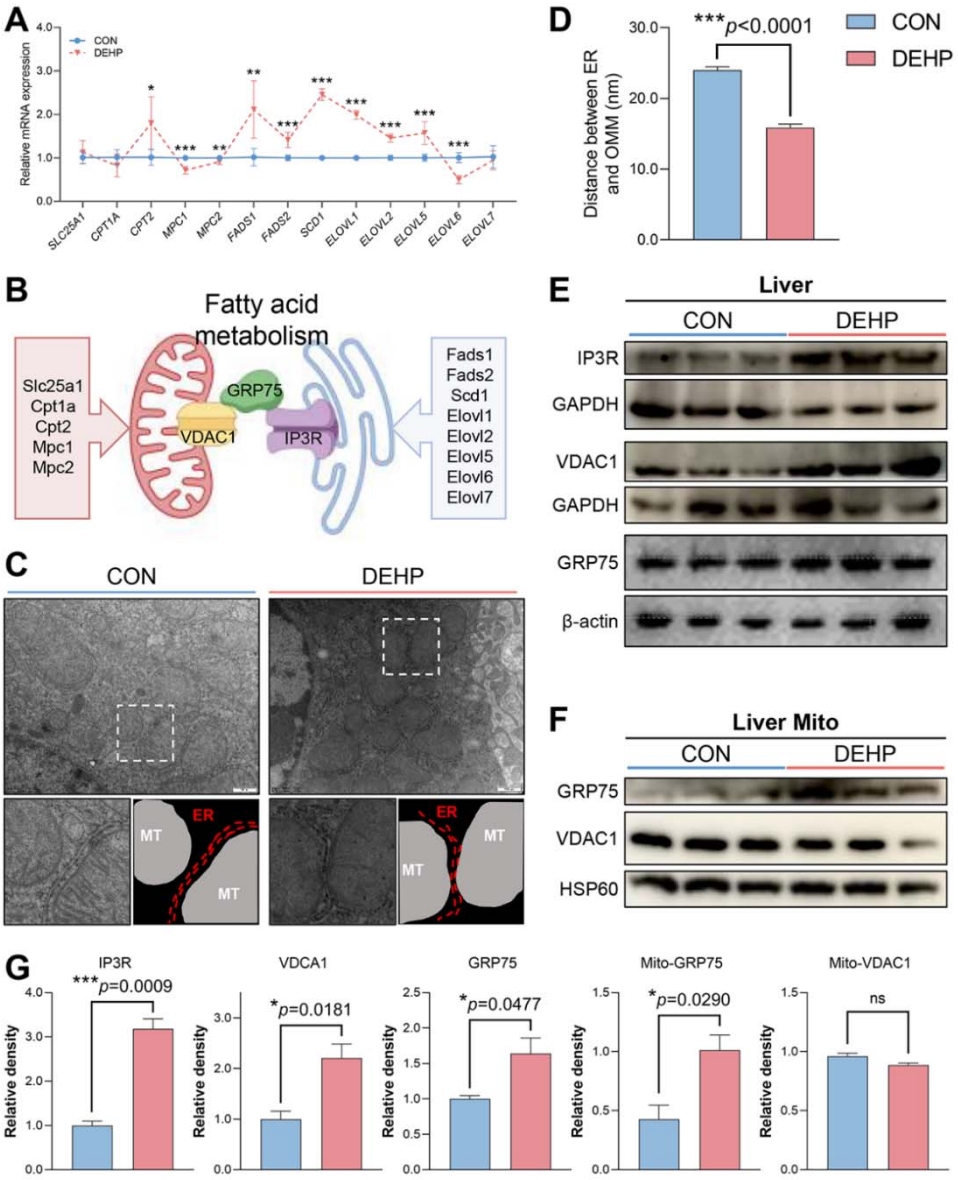

Figure 4. DEHP causes the increase in MAM formation. (A) Expression of mRNA of fatty acid metabolism related gene. *n=6*. (B) Schematic diagram of the relationship between MAMs and fatty acid metabolism. (C) Transmission electron microscopy of livers. Insets are mitochondrial membrane (dark gray) and ER membrane (red) annotated with different colors. (D) The distance between ER and OMM (n = 45 mitochondria). (E) Levels of MAMs-related proteins in mouse livers; GAPDH or β-actin served as loading controls for the total fraction. *n=3*. (F) Levels of MAMs-related proteins in mouse liver mitochondria; HSP60 served as loading controls for the total fraction. *n=3*. (G) Relative IP3R, VDAC1 and GRP75 content in mouse liver. Relative VDAC1 and GRP75 content in mouse liver mitochondria. *n=3*. Data are presented as the mean ± SD, $n \geq 3$. Symbol for the significance of differences between the CON group and another group: $^{*}P < 0.05$, $^{***}P < 0.001$.

3.5. MEHP resulted in increased MAMs and promoted lipid deposition in AML12 cells

DEHP undergoes rapid metabolism to form MEHP within the murine liver[10]. To further assess the effects of DEHP on hepatocytes, AML12 cells were subjected to *in vitro* treatment with MEHP at concentrations of 50, 100, and 200 μmol/L (Figure 5A and S1). The outcomes of *in vivo* experiments and Nile red staining were in agreement. AML12 cells develop lipid accumulation as a result of MEHP (Figure 5B). In AML12 cells of the M200 group, the expression levels of PLIN2 and HSC70 proteins increased significantly (Figures 5C-D). Following mitochondrial impairment, changes in the mitochondrial membrane architecture are triggered. We assessed the MMP, and our findings indicate that MEHP induced modifications in the MMP

of AML12 cells, as shown in Figure 6A. By examining the ER and mitochondrial binding in AML12 cells, we assessed the formation of MAM. Enhanced ER-mitochondria co-localization was observed in MEHP-treated AML12 cells, confirmed via IF staining and Pearson correlation coefficient analysis (Figure 5B). Phosphofurin acidic cluster-sorting protein 2 (PACS2) is an essential protein molecule for performing MAM ligation and maintaining the stability of MAM[41]. MAM contains numerous proteins associated with lipid metabolism, which are vital for lipid synthesis and transfer. Notably, DGAT2 serves as a critical enzyme in TG synthesis, while ACAT1 is essential for cholesterol synthesis. In our study, we assessed the MAM-related protein levels of AML12 cells treated with MEHP. Exposure to MEHP led to the upregulation of multiple proteins implicated in MAM formation, including ACAT1, PACS2, DGAT2, GRP75, and VDAC1 (Figures 5C-D). These results indicated that MEHP leads to an increase in MAM formation and promotes lipid deposition in AML12 cells.

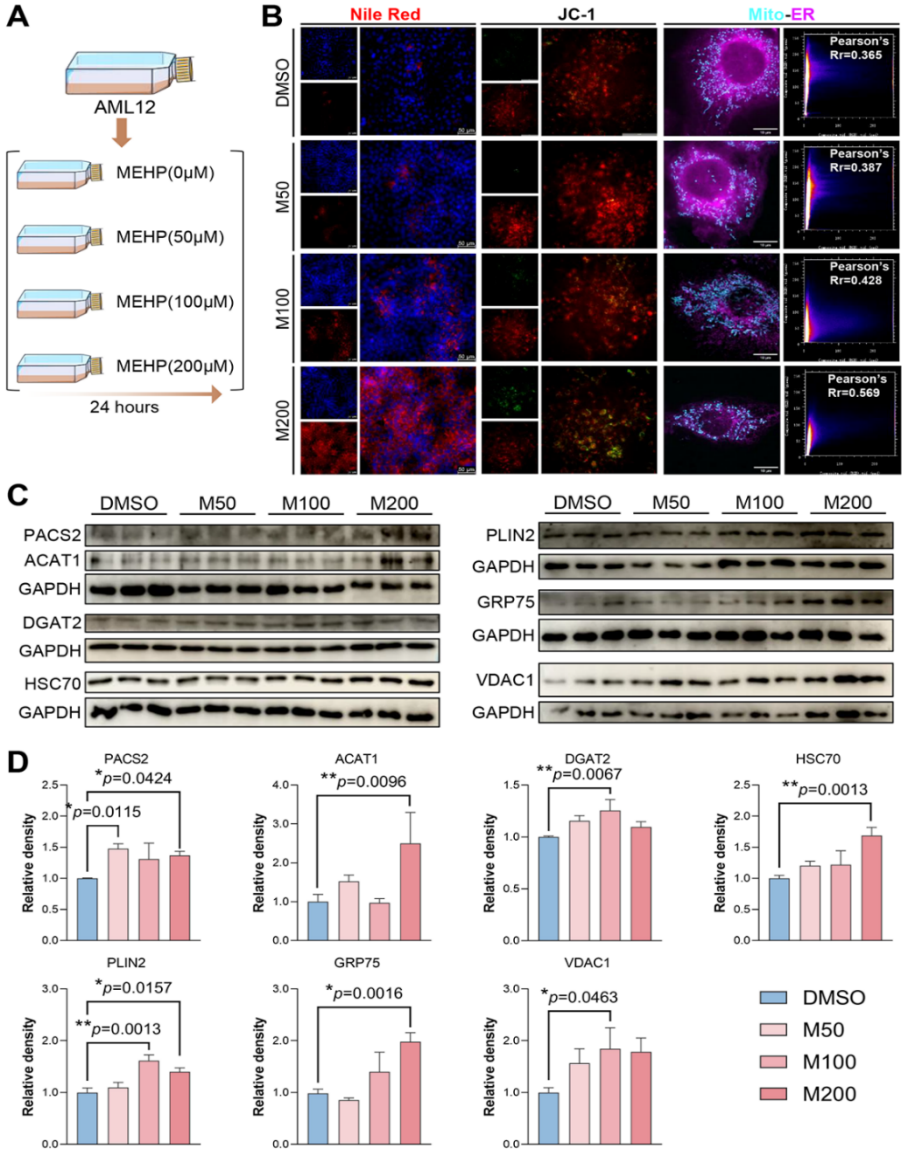

Figure 5. Exposure to MEHP triggers the formation of MAMs and lipid accumulation in AML12 cells. (A) AML12 cells were incubated with MEHP (0, 50, 100, and 200 μmol/L)). (B) IF analysis of lipid droplet distribution, MMP, and ER-mitochondria co-localization in AML12 cells. (C) Levels of MAMs and lipid metabolism-related proteins in AML12 cells; GAPDH served as loading controls for the total fraction. (D) Relative PACS2, ACAT1, DGAT2, HSC70, PLIN2, GRP75, and VDAC1 content in AML12 cells. Data are presented as the mean ± SD, $n \geq 3$. Symbol for the significance of differences between the CON group and another group: $^{*}P < 0.05$, $^{**}P < 0.01$.

3.6. Knockdown of GRP75 to reduce MAMs can inhibit MEHP-induced lipid deposition

GRP75 exists in MAM and plays a core role in constructing protein complexes with IP3R and VDAC1[24]. PPI network analysis revealed that lipid metabolism was associated with MAM formation, suggesting that GRP75 played an important role (Figure 6A). To determine the key role of GRP75, we conducted subsequent experiments using GRP75 siRNA and 200 μmol/L MEHP. After MEHP treatment, the level of GRP75 protein in AML12 cells significantly increased, and returned to normal after combined treatment with siGRP75 (Figures 6C-D). siGRP75 can alleviate the increased expression of PACS2, DGAT2, PLIN2 and HSC70 induced by MEHP. In addition, knocking down GRP75 weakens the effects of lipid deposition, MMP damage, and MAM formation caused by MEHP (Figure 6B). These results indicate that GRP75 is the core molecule by which MEHP disrupts lipid homeostasis in AML2 cells. Knockdown of GRP75 can effectively alleviate lipid deposition and related organelle dysfunction caused by MEHP.

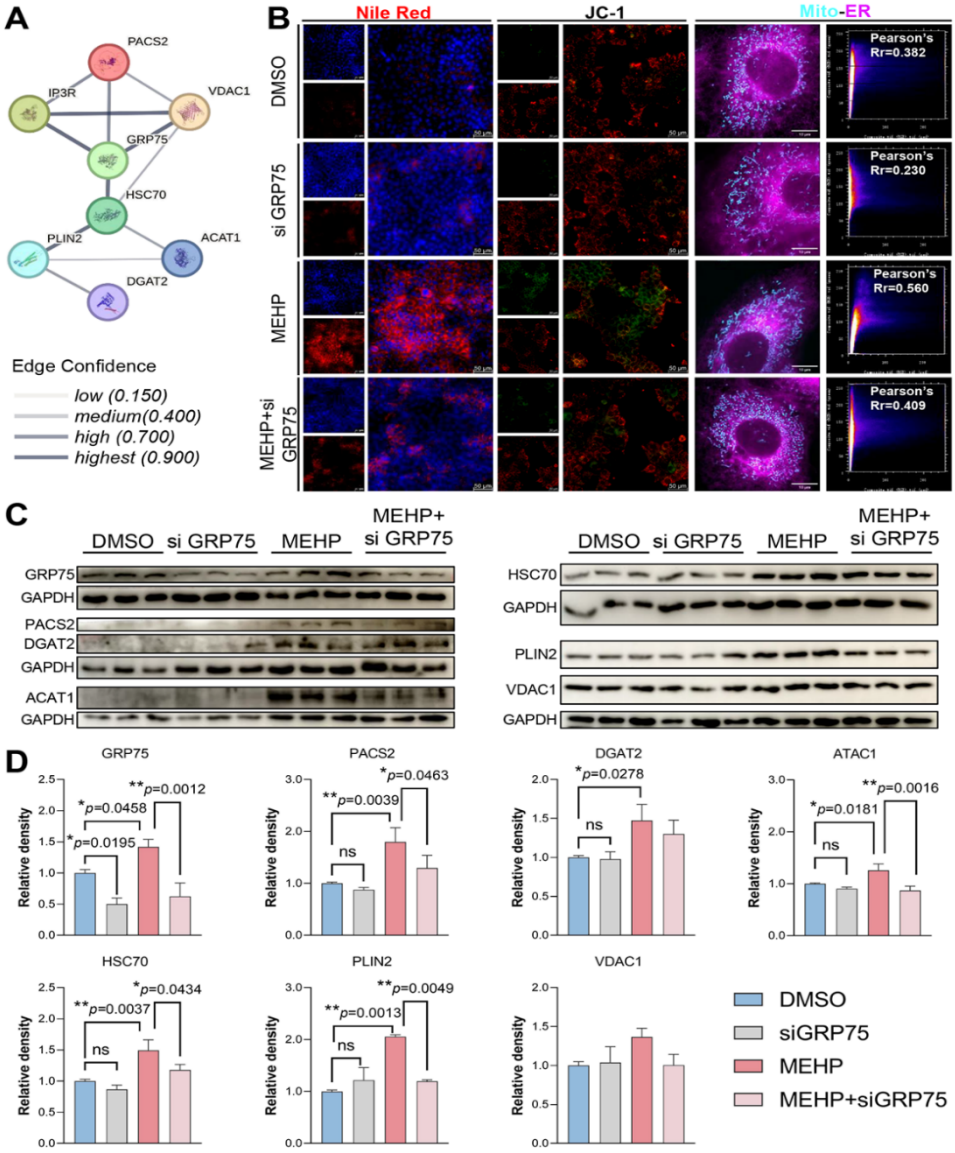

Figure 6. Knockdown of GRP75 to reduce MAMs can inhibit MEHP-induced lipid deposition in AML12 cells. (A) PPI network of MAMs and lipid droplets. (B) IF analysis of lipid droplet distribution, MMP, and ER-mitochondria co-localization in AML12 cells. (C) Levels of MAMs and lipid metabolism-related proteins in AML12 cells; GAPDH served as loading controls for the total fraction. (D) Relative GRP75, PACS2, DGAT2, ACAT1, HSC70, PLIN2, and VDAC1 content in AML12 cells. Data are presented as the mean ± SD, $n \geq 3$. Symbol for the significance of differences between the CON group and another group: $^{*}P < 0.05$, $^{**}P < 0.01$.

3.7. MEHP induced lipid accumulation in AML12 cells by targeting GRP75

To clarify the sufficiency and direct role of GRP75 in MEHP-induced lipid deposition, we constructed an AML12 cell model with overexpression of GRP75 for functional gain studies (Figures 7A, C). The results indicated that overexpression of GRP75 upregulated the expression of PLIN2 and HSC70 (Figure 7A, C). Consistent with these findings, intracellular lipid deposition was significantly increased, as demonstrated by Oil Red O and Nile Red staining (Figure 7B-C). This confirms the crucial role of GRP75 in driving lipid accumulation in AML12 cells. It is worth noting that when cells overexpressing GRP75 were further treated with MEHP, the degree of lipid deposition was more severe than that in the group with overexpression alone (Figure 7B-C). The result suggests that in addition to exerting its effect through GRP75, MEHP may also use other pathways that exacerbate lipid metabolism disorders. To directly verify whether MEHP targets the GRP75 protein, molecular docking simulations, CETSA, and DARTS experiments were performed. Molecular docking simulations have demonstrated that MEHP molecules possess the ability to penetrate significantly into the active sites of the GRP75 protein. Their binding is mainly driven by hydrophobic interactions (involving residues such as CYS317 and MET389), and they form key hydrogen bond networks with multiple residues, including GLY388 and ASN64 (Figure 7D). The binding free energy calculated by Molecular Mechanics Generalized Born Surface Area (MM-GBSA) was -30.78 kcal/mol. It indicates that the combination of the two is stable and has a strong affinity. The results of CETSA showed that MEHP treatment significantly improved the thermal stability of the GRP75 protein (Figure 7E). Meanwhile, the results of DARTs demonstrated that MEHP could protect GRP75 from protease hydrolysis (Figure 7F). The results of DARTS and CETSA complement each other, confirming that MEHP directly binds to and stabilizes the GRP75 protein. These results indicate that MEHP increases MAM formation by directly targeting GRP75, which subsequently disrupts fatty acid metabolism and ultimately leads to lipid deposition in hepatocytes.

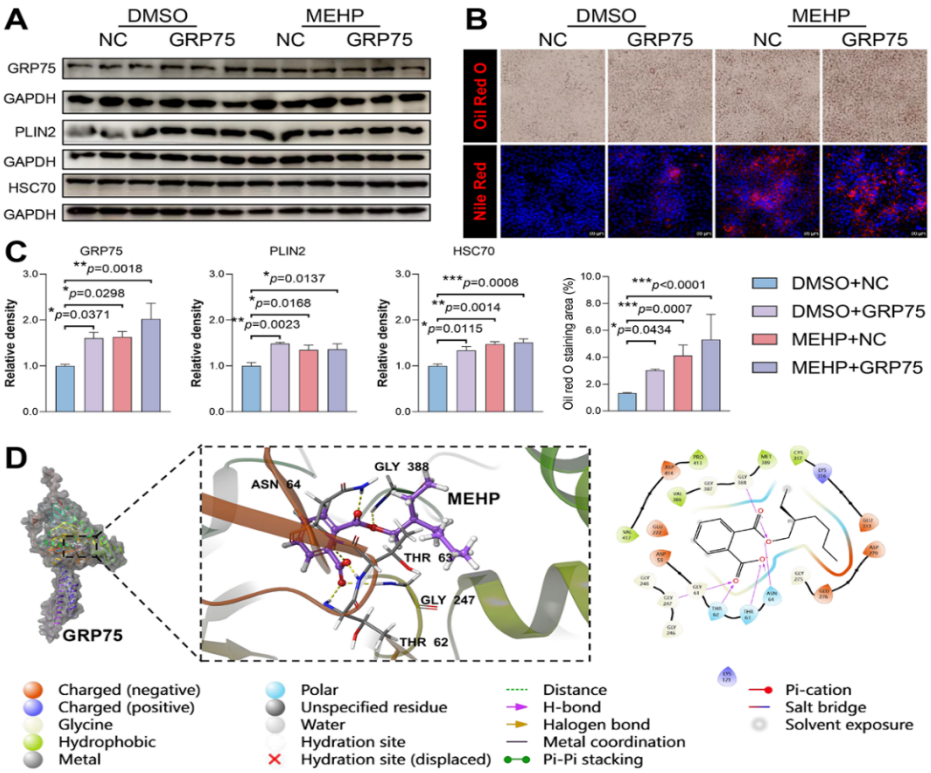

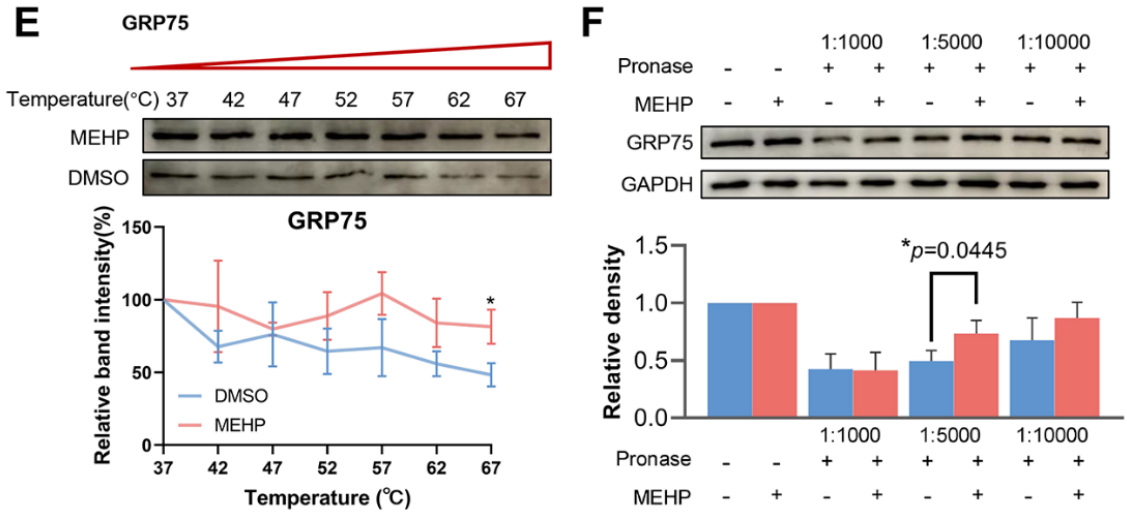

Figure 7. MEHP induces lipid accumulation in AML12 cells by targeting GRP75. (A) Levels of lipid droplets-related proteins in AML12 cells; GAPDH served as loading controls for the total fraction. (B) Oil Red O staining and lipid droplets in AML12 cells. (C) Relative GRP75, PLIN2, and HSC70 content in AML12 cells. Quantification of Oil Red O staining. (D) Molecular docking simulation for the ligand-protein binding of MEHP with GRP75. (E) CETSA presented the thermal stability of GRP75 proteins after treatment with MEHP (200 μmol/L). (F) DARTs was performed in MEHP induced AML12 cells treated with 200 μmol/L). Data are presented as the mean ± SD, $n \geq 3$. Symbol for the significance of differences between the CON group and another group: $^{*}P < 0.05$, $^{**}P < 0.01$, and $^{***}P < 0.001$.

4. Discussion

Phthalates, recognized as a category of endocrine-disrupting chemicals with potential hepatotoxicity, have emerged as a considerable public health concern[42, 43]. Among these, with its high persistence, DEHP is the most common phthalate found in the environment. It has been listed as a priority hazardous pollutant worldwide[44, 45]. Although there is evidence suggesting that DEHP exposure is related to liver lipid metabolism disorders, the mechanism of MAMs in this pathological process has not yet been explored. The mechanism of DEHP-induced hepatotoxicity was further examined in this work, and it was found that DEHP exposure caused damage to liver structure and function in mice through the excessive formation of MAM. The findings of our research results indicate that MEHP, the principal bioactive metabolite of DEHP, enhances the stability of MAM by up-regulating GRP75, thereby promoting lipid accumulation. Crucially, GRP75 knockdown and overexpression experiments demonstrated the key regulatory role of this molecular pathway in alleviating MEHP-induced steatosis. These results identified GRP75 as a positive regulator of MEHP-induced lipid deposition and also positioned MAM kinetics as a key link between environmental pollutant exposure and metabolic liver diseases.

Hepatic lipid deposition is one of the most common causes of chronic liver disease (NAFLD)[46]. The findings of our study demonstrate that DEHP exposure leads to liver injury and metabolic disturbances in lipid homeostasis. Histopathological analysis revealed that DEHP led to structural disorder and vacuolation of mouse hepatocytes, accompanied by elevated serum biomarkers (AST/ALT, ALP, and CHE), indicating hepatocyte injury and functional impairment. Notably, DEHP exposure promoted hepatic lipid accumulation, demonstrated by Oil Red O staining and by ultrastructural confirmation of elevated lipid droplets. This phenotype was further supported by the elevated levels of serum TC, LDL-C, and HDL-C, as well as the upregulation of PLIN2 (a key regulator of lipid droplet stability) expression. KEGG pathway analysis of

differential metabolites revealed a coordinated disruption in lipid, protein, and carbohydrate metabolism, implicating a systemic disturbance of the hepatic metabolic network by DEHP. Among them, lipid metabolism pathways, especially fatty acid degradation, sphingolipid metabolism, and NAFLD pathways, are most significantly affected. The liver can directly participate in the synthesis and decomposition of fatty acids. Metabolomics analysis has revealed that DEHP causes disorders in liver fatty acid metabolism, primarily characterized by changes in glycerol, citric acid cycles, and fatty acid-related metabolites. Focused analysis of lipid differential metabolites revealed that the levels of TG and its synthetic precursor LysoPA significantly increased, while the key phospholipid PG on the mitochondrial membrane was downregulated. After DEHP exposure, the activity of DGAT2, a key enzyme that catalyzes TG synthesis in the liver, was enhanced, while the efficiency of FAO, which reflects the mitochondrial FAO capacity, was significantly weakened. This imbalance in fatty acid metabolism leads to excessive hepatic lipid accumulation.

MAMs serve as critical centers for lipid synthesis, transport, and FAO[17]. Mechanistically, DEHP-induced metabolic disorders are mediated by MAM dysfunction, which is driven by its promotion of excessive MAM formation[47]. Under electron microscopy, it was observed that the ER-mitochondrial contact distance shortened and the expression of MAM conjunctional proteins (IP3R1, GRP75, VDAC1) increased. This structural remodeling is consistent with the changes in the mRNA levels of genes related to fatty acid metabolism (such as CPT1A, SCD1, and ELOVLs), indicating that MAMs play a key role in the lipid imbalance induced by DEHP. These findings were confirmed in AML12 hepatocytes, where the main metabolite of DEHP, MEHP, reproduced *in vivo* phenotypes: dose-dependent lipid accumulation, MMP depolarization, and enhanced MAM formation. Furthermore, MEHP treatment upregulated key proteins within MAMs, including lipid-synthesizing enzymes (DGAT2, ACAT1) and the structural regulator PACS2, which is critical for MAM stability. This establishes a direct link between MAM formation and the generation of lipid, thereby reinforcing the causal relationship between MAM dynamics and lipid accumulation.

The structural integrity of MAMs is meticulously regulated by GRP75[24]. This study confirmed the pivotal position of GRP75 in DEHP-induced hepatotoxicity through functional gain and loss experiments. GRP75 knockdown can effectively alleviate the excessive formation of MAMs and lipid deposition induced by MEHP. In contrast, GRP75 overexpression led to a synergistic exacerbation of MEHP-induced lipid accumulation. This discovery suggests that GRP75 is a positive regulatory factor for MEHP-induced hepatic steatosis. This finding aligns with previous research indicating GRP75 overexpression enhances the stability of MAM, thereby promoting lipid transfer between mitochondria and ER[17, 40]. However, overexpression experiments also suggest that, apart from the GRP75-MAMs axis, there may be other parallel pathways involved in the hepatotoxic effects of DEHP. Existing evidence indicates that DEHP and MEHP can interfere with peroxisome proliferator-activated receptors (PPAR) and are likely to initiate the above-mentioned metabolic disorders by interfering with the PPAR signaling pathway[48]. PPARα and PPARγ are the central regulators of lipid metabolism. DEHP/MEHP can activate PPARγ, thereby driving lipid accumulation[49]. More importantly, the latest research indicates that the activity of PPARα is directly related to the abundance

and function of MAMs[50]. Therefore, DEHP may disrupt the metabolic homeostasis of hepatocytes by interfering with the balance of PPARα/γ, initiating abnormal expression of downstream lipid metabolite-related genes, and cooperatively regulating the assembly of MAMs.

Abnormal formation and functional disorder of MAMs have multi-dimensional consequences. MAMs are key nodes for regulating intracellular calcium (Ca^{2+}) signaling and the balance of reactive oxygen species (ROS)[51]. Also, the upregulation of MAMs may lead to mitochondrial Ca^{2+} overload, which in turn disrupts the electron transport chain, intensifies ROS production, and induces a decrease in MMP[52]. The resultant oxidative stress and Ca^{2+} homeostasis imbalance can further damage mitochondrial function, inhibit FAO, and activate inflammatory and apoptotic pathways, thereby forming a vicious cycle with lipid accumulation that synergistically aggravates hepatic damage.

To detect the molecular level how MEHP regulates GRP75, we conducted computer simulations and biophysical experiments. Molecular docking revealed that MEHP stably binds within the substrate-binding pocket of GRP75, primarily through the formation of multiple hydrogen bonds and hydrophobic interactions. The binding free energy is -30.78 kcal/mol, indicating high binding affinity. CETSA and DARTs experiments further confirmed the direct binding of MEHP and GRP75 within cells. Our findings suggest that DEHP/MEHP upregulates GRP75 expression, which promotes excessive MAM formation. This, in turn, disrupts the balance between fatty acid synthesis and catabolism, thereby creating a favorable microenvironment for hepatic steatosis.

Although this study identified MAM dysregulation as the central pathway of DEHP hepatotoxicity, there are still several issues that require further research. Firstly, the chosen dose of DEHP (200 mg/kg/day) is reasonable in the study of toxicological mechanisms. However, it is higher than the average person's exposure to the environment through food, water, or air. Therefore, in the future, studies on lower doses and long-term exposures as well as epidemiological data will be needed to supplement and verify. Secondly, it has been reported that DEHP exposure in developing quail can interfere with liver CYP450 metabolism, suggesting that the liver is particularly sensitive to DEHP during development[53]. It is necessary to further verify the specific susceptibility of developmental stages through age comparison experiments. Finally, the specific details of DEHP/MEHP regulating MAMs through PPAR signaling and influencing calcium homeostasis/oxidative stress through MAMs still require in-depth research.

5. Conclusion

In conclusion, our study elucidates a mechanism involving GRP75, whereby DEHP disrupts liver lipid homeostasis by promoting the excessive formation of MAMs. These findings not only deepen our understanding of environmental liver toxins but also highlight the GRP75 and MAM-related pathways are promising therapeutic targets for chemically induced metabolic liver diseases. Future research should explore the applicability of these mechanisms to other phthalates and evaluate their persistence models of human exposure.

Availability of data and materials

The corresponding author will provide the datasets used and/or analyzed during the current work upon reasonable request.

Declaration of competing interest

The authors claim that there are no conflicting interests.

Acknowledgments

This study has received assistance from National Natural Science Foundation of China (No.32302934 and No. 32172932), China Agriculture Research System of MOF and MARA (No. CARS-35). We thank BioRender website (app.biorender.com) for schematic diagrams and graphical abstract framing.

References

[1] J. Eales, A. Bethel, T. Galloway, et al., Human health impacts of exposure to phthalate plasticizers: An overview of reviews, Environ Int. 158 (2022) 106903. https://doi.org/10.1016/j.envint.2021.106903.

[2] Z. Wen, Y. Xie, M. Chen, et al., China's plastic import ban increases prospects of environmental impact mitigation of plastic waste trade flow worldwide, Nat Commun. 12 (2021) 425. https://doi.org/10.1038/s41467-020-20741-9.

[3] K. Kaur, S. Reddy, P. Barathe, et al., Microplastic-associated pathogens and antimicrobial resistance in environment, Chemosphere. 291 (2022) 133005. https://doi.org/10.1016/j.chemosphere.2021.133005.

[4] X. Xu, Y. He, Z. Cheng, et al., Environmental endocrine disrupting chemical-DEHP exposure-provoked biotoxicity about microbiota-gut-mammary axis in lactating mice via multi-omics technologies, Environ Int. 193 (2024) 109130. https://doi.org/10.1016/j.envint.2024.109130.

[5] X. Zhang, W. Qi, Q. Xu, et al., Di(2-ethylhexyl) phthalate (DEHP) and thyroid: biological mechanisms of interference and possible clinical implications, Environ Sci Pollut Res Int. 29 (2022) 1634-1644. https://doi.org/10.1007/s11356-021-17027-y.

[6] T. Fierens, M. Van Holderbeke, H. Willems, et al., Transfer of eight phthalates through the milk chain--a case study, Environ Int. 51 (2013) 1-7. https://doi.org/10.1016/j.envint.2012.10.002.

[7] X. Zhang, M. Wu, Z. Liu, et al., Increasing prevalence of NAFLD/NASH among children, adolescents and young adults from 1990 to 2017: a population-based observational study, BMJ Open. 11 (2021) e042843. https://doi.org/10.1136/bmjopen-2020-042843.

[8] W. Li, H. Xiao, H. Wu, et al., Analysis of environmental chemical mixtures and nonalcoholic fatty liver disease: NHANES 1999-2014, Environ Pollut. 311 (2022) 119915. https://doi.org/10.1016/j.envpol.2022.119915.

[9] S. Cai, J. Fan, J. Ye, et al., Phthalates exposure is associated with non-alcoholic fatty liver disease among US adults, Ecotoxicol Environ Saf. 224 (2021) 112665. https://doi.org/10.1016/j.ecoenv.2021.112665.

[10] H. Zhang, J.G. Cui, M.S. Chen, et al., TNF/TNFR1 Signaling Mediates DEHP-Induced Hepatocyte Pyroptosis via the GSDMD-mtROS Axis, J Agric Food Chem. (2025) https://doi.org/10.1021/acs.jafc.4c11022.

[11] Y. Zhao, J.G. Cui, H. Zhang, et al., Role of mitochondria-endoplasmic reticulum coupling in lycopene preventing DEHP-induced hepatotoxicity, Food Funct. 12 (2021) 10741-10749. https://doi.org/10.1039/d1fo00478f.

[12] X. Du, D.L. Li, X. Xu, et al., Effects of mixed exposure to PFAS on adolescent non-alcoholic fatty liver disease: Integrating evidence from human cohorts, toxicogenomics, and animal models to uncover mechanisms and potential target sites, J Hazard Mater. 485 (2025) 136854. https://doi.org/10.1016/j.jhazmat.2024.136854.

[13] M. Averina, J. Brox, S. Huber, et al., Exposure to perfluoroalkyl substances (PFAS) and dyslipidemia, hypertension and obesity in adolescents. The Fit Futures study, Environ Res. 195 (2021) 110740. https://doi.org/10.1016/j.envres.2021.110740.

[14] U. Heudorf, V. Mersch-Sundermann, J. Angerer, Phthalates: toxicology and exposure, Int J Hyg Environ Health. 210 (2007) 623-634. https://doi.org/10.1016/j.ijheh.2007.07.011.

[15] M. Alves-Bezerra, D.E. Cohen, Triglyceride Metabolism in the Liver, Compr Physiol. 8 (2017) 1-8.

https://doi.org/10.1002/cphy.c170012.

[16] P. Nguyen, V. Leray, M. Diez, et al., Liver lipid metabolism, J Anim Physiol Anim Nutr (Berl). 92 (2008) 272-283. https://doi.org/10.1111/j.1439-0396.2007.00752.x.

[17] S. Bathina, U.N. Das, Role of Mitochondrial Dysfunction in Cellular Lipid Homeostasis and Disease, Discov Med. 35 (2023) 653-663. https://doi.org/10.24976/Discov.Med.202335178.64.

[18] S. Tian, P. Lei, J. Zhang, et al., Sulforaphane Balances Ca(2+) Homeostasis Injured by Excessive Fat via Mitochondria-Associated Membrane (MAM), Mol Nutr Food Res. 65 (2021) e2001076. https://doi.org/10.1002/mnfr.202001076.

[19] A. Bassot, C. Prip-Buus, A. Alves, et al., Loss and gain of function of Grp75 or mitofusin 2 distinctly alter cholesterol metabolism, but all promote triglyceride accumulation in hepatocytes, Biochim Biophys Acta Mol Cell Biol Lipids. 1866 (2021) 159030. https://doi.org/10.1016/j.bbalip.2021.159030.

[20] S. Tian, P. Lei, C. Teng, et al., Targeting PLIN2/PLIN5-PPARgamma: Sulforaphane Disturbs the Maturation of Lipid Droplets, Mol Nutr Food Res. 63 (2019) e1900183. https://doi.org/10.1002/mnfr.201900183.

[21] K. Peng, S. Wang, R. Liu, et al., Effects of UBE3A on Cell and Liver Metabolism through the Ubiquitination of PDHA1 and ACAT1, Biochemistry. 62 (2023) 1274-1286. https://doi.org/10.1021/acs.biochem.2c00624.

[22] S. Rong, M. Xia, G. Vale, et al., DGAT2 inhibition blocks SREBP-1 cleavage and improves hepatic steatosis by increasing phosphatidylethanolamine in the ER, Cell Metab. 36 (2024) 617-629 e617. https://doi.org/10.1016/j.cmet.2024.01.011.

[23] R.A. Calle, N.B. Amin, S. Carvajal-Gonzalez, et al., ACC inhibitor alone or co-administered with a DGAT2 inhibitor in patients with non-alcoholic fatty liver disease: two parallel, placebo-controlled, randomized phase 2a trials, Nat Med. 27 (2021) 1836-1848. https://doi.org/10.1038/s41591-021-01489-1.

[24] J. Li, F. Qi, H. Su, et al., GRP75-faciliated Mitochondria-associated ER Membrane (MAM) Integrity controls Cisplatin-resistance in Ovarian Cancer Patients, Int J Biol Sci. 18 (2022) 2914-2931. https://doi.org/10.7150/ijbs.71571.

[25] Y. Lv, L. Cheng, F. Peng, Compositions and Functions of Mitochondria-Associated Endoplasmic Reticulum Membranes and Their Contribution to Cardioprotection by Exercise Preconditioning, Front Physiol. 13 (2022) 910452. https://doi.org/10.3389/fphys.2022.910452.

[26] Y.F. Song, Z.Y. Bai, X.H. Lai, et al., Ip3r-Grp75-Vdac and Relevant Ca(2+) Signaling Regulate Dietary Palmitic Acid-Induced De Novo Lipogenesis by Mitochondria-Associated ER Membrane (MAM) Recruiting Seipin in Yellow Catfish, J Nutr. (2024) https://doi.org/10.1016/j.tjnut.2024.04.021.

[27] J. Wang, Y. Wei, Y. Wu, et al., Di-(2-ethylhexyl) phthalate induces prepubertal testicular injury through MAM-related mitochondrial calcium overload in Leydig and Sertoli cell apoptosis, Toxicology. 509 (2024) 153956. https://doi.org/10.1016/j.tox.2024.153956.

[28] K. Becker, M. Seiwert, J. Angerer, et al., DEHP metabolites in urine of children and DEHP in house dust, Int J Hyg Environ Health. 207 (2004) 409-417. https://doi.org/10.1078/1438-4639-00309.

[29] J.G. Cui, H. Zhang, Y.Q. Zhang, et al., A new insight into the mechanism of DEHP-induced cardiotoxicity: Triggering pyroptosis of cardiomyocytes by disrupting sphingolipid metabolism, J Hazard Mater. 499 (2025) 140148. https://doi.org/10.1016/j.jhazmat.2025.140148.

[30] M.L. Sassano, Y.Y. Tyurina, A. Diokmetzidou, et al., Endoplasmic reticulum-mitochondria contacts are prime hotspots of phospholipid peroxidation driving ferroptosis, Nat Cell Biol. 27 (2025) 902-917. https://doi.org/10.1038/s41556-025-01668-z.

[31] J. Dong, L. Chen, F. Ye, et al., Mic19 depletion impairs endoplasmic reticulum-mitochondrial contacts and mitochondrial lipid metabolism and triggers liver disease, Nat Commun. 15 (2024) 168. https://doi.org/10.1038/s41467-023-44057-6.

[32] C. Wang, X. Dai, S. Wu, et al., FUNDC1-dependent mitochondria-associated endoplasmic reticulum membranes are involved in angiogenesis and neoangiogenesis, Nat Commun. 12 (2021) 2616. https://doi.org/10.1038/s41467-021-22771-3.

[33] T.H. Tsai, E. Chen, L. Li, et al., The constitutive lipid droplet protein PLIN2 regulates autophagy in liver, Autophagy. 13 (2017) 1130-1144. https://doi.org/10.1080/15548627.2017.1319544.

[34] L. Hu, D. Tang, B. Qi, et al., Mfn2/Hsc70 Complex Mediates the Formation of Mitochondria-Lipid Droplets Membrane Contact and Regulates Myocardial Lipid Metabolism, Adv Sci (Weinh). 11 (2024) e2307749. https://doi.org/10.1002/advs.202307749.

[35] M.A. Blaskovich, V. Yendluri, H.R. Lawrence, et al., Lysophosphatidic acid acyltransferase beta regulates mTOR signaling, PLoS One. 8 (2013) e78632. https://doi.org/10.1371/journal.pone.0078632.

[36] H. Sun, J. Zhang, Q. Ye, et al., LPGAT1 controls MEGDEL syndrome by coupling phosphatidylglycerol remodeling with mitochondrial transport, Cell Rep. 42 (2023) 113214. https://doi.org/10.1016/j.celrep.2023.113214.

[37] M.J. Akhtar, S.A. Khan, B. Kumar, et al., Role of sodium dependent SLC13 transporter inhibitors in various metabolic disorders, Mol Cell Biochem. 478 (2023) 1669-1687. https://doi.org/10.1007/s11010-022-04618-7.

[38] M. Kerr, M.S. Dodd, L.C. Heather, The 'Goldilocks zone' of fatty acid metabolism; to ensure that the relationship with cardiac function is just right, Clin Sci (Lond). 131 (2017) 2079-2094. https://doi.org/10.1042/CS20160671.

[39] M. Yue, B. Hu, J. Li, et al., Coronaviral ORF6 protein mediates inter-organelle contacts and modulates host cell lipid flux for virus production, EMBO J. 42 (2023) e112542. https://doi.org/10.15252/embj.2022112542.

[40] Y.J. Chi, Z.Y. Bai, G.L. Feng, et al., ER-mitochondria contact sites regulate hepatic lipogenesis via Ip3r-Grp75-Vdac complex recruiting Seipin, Cell Commun Signal. 22 (2024) 464. https://doi.org/10.1186/s12964-024-01829-x.

[41] J. Yang, M. Sun, R. Chen, et al., Mitochondria-associated membrane protein PACS2 maintains right cardiac function in hypobaric hypoxia, iScience. 26 (2023) 106328. https://doi.org/10.1016/j.isci.2023.106328.

[42] Z.B. Zhao, K. Ji, X.Y. Shen, et al., Di(2-ethylhexyl) phthalate promotes hepatic fibrosis by regulation of oxidative stress and inflammation responses in rats, Environ Toxicol Pharmacol. 68 (2019) 109-119. https://doi.org/10.1016/j.etap.2019.03.008.

[43] R.K. Morgan, K. Wang, L.K. Svoboda, et al., Effects of Developmental Lead and Phthalate Exposures on DNA Methylation in Adult Mouse Blood, Brain, and Liver: A Focus on Genomic Imprinting by Tissue and Sex, Environ Health Perspect. 132 (2024) 67003. https://doi.org/10.1289/EHP14074.

[44] X. Xie, Z. Wang, X. Zhou, et al., Study on the interaction of phthalate esters to human serum albumin by steady-state and time-resolved fluorescence and circular dichroism spectroscopy, J Hazard Mater. 192 (2011) 1291-1298. https://doi.org/10.1016/j.jhazmat.2011.06.038.

[45] J.G. Cui, H. Zhang, M.S. Chen, et al., Lycopene Prevents DEHP-Induced Ferroptosis in Cerebellar Microglia by Regulating the PEBP1/ALOX15 Axis, J Agric Food Chem. (2026) https://doi.org/10.1021/acs.jafc.5c08862.

[46] A.A.-S. G, M.A.-M. G, R. Tamrakar, et al., Fasting, Nutrition and Weight Loss: An Approach to Refine Non-Alcoholic Fatty Liver Disease, J Nutr Sci Vitaminol (Tokyo). 67 (2021) 366-374. https://doi.org/10.3177/jnsv.67.366.

[47] Y. Zhao, Y.H. Chang, H.R. Ren, et al., Phthalates Induce Neurotoxicity by Disrupting the Mfn2-PERK Axis-Mediated Endoplasmic Reticulum-Mitochondria Interaction, J Agric Food Chem. 72 (2024) 7411-7422. https://doi.org/10.1021/acs.jafc.3c07752.

[48] R.L. Melnick, Is peroxisome proliferation an obligatory precursor step in the carcinogenicity of di(2-ethylhexyl)phthalate (DEHP)?, Environ Health Perspect. 109 (2001) 437-442. https://doi.org/10.1289/ehp.01109437.

[49] Y. Zhao, D.X. Ma, H.G. Wang, et al., Lycopene Prevents DEHP-Induced Liver Lipid Metabolism Disorder by Inhibiting the HIF-1alpha-Induced PPARalpha/PPARgamma/FXR/LXR System, J Agric Food Chem. 68 (2020) 11468-11479. https://doi.org/10.1021/acs.jafc.0c05077.

[50] H. Kim, Q. Chen, D. Ju, et al., ER-tethered stress sensor CREBH regulates mitochondrial unfolded protein response to maintain energy homeostasis, Proc Natl Acad Sci U S A. 121 (2024) e2410486121. https://doi.org/10.1073/pnas.2410486121.

[51] S. Missiroli, S. Patergnani, N. Caroccia, et al., Mitochondria-associated membranes (MAMs) and inflammation, Cell Death Dis. 9 (2018) 329. https://doi.org/10.1038/s41419-017-0027-2.

[52] W. Chen, Z. Shen, W. Dong, et al., Polygonatum sibiricum polysaccharide ameliorates skeletal muscle aging via mitochondria-associated membrane-mediated calcium homeostasis regulation, Phytomedicine. 129 (2024) 155567. https://doi.org/10.1016/j.phymed.2024.155567.

[53] Y.Z. Zhang, Y.Z. Zuo, Z.H. Du, et al., Di (2-ethylhexyl) phthalate (DEHP)-induced hepatotoxicity in quails (Coturnix japonica) via triggering nuclear xenobiotic receptors and modulating cytochrome P450 systems, Food Chem Toxicol. 120 (2018) 287-293. https://doi.org/10.1016/j.fct.2018.07.019.